



Contents lists available at ScienceDirect

Opto-Electronics Review

journal homepage: <http://www.journals.elsevier.com/pto-electronics-review>

Discontinuity of dipole-moment matrix elements in ellipsoidally shaped nanoparticles and profiles of spectral lines

T. Kereselidze^{a,*}, T. Tchelidze^a, A. Devdariani^b^a Faculty of Exact and Natural Sciences, Tbilisi State University, 1 Chavchavadze Ave., 0179 Tbilisi, Georgia^b St. Petersburg State University, 11/2 Lieutenant Schmidt Emb., St. Petersburg 199034, Russia

ARTICLE INFO
Article history:

Received 11 February 2018

Received in revised form 25 February 2018

Accepted 27 February 2018

Available online 26 April 2018

Keywords:

Nanoparticle

Ellipsoidal shape

Shape-anisotropy parameter

Profile of spectral line

ABSTRACT

The behaviour of energy levels and optical spectra of a charged particle (electron or hole) confined within a potential well of ellipsoidal shape is investigated as a function of the shape-anisotropy parameter. If two energy levels of the same symmetry intersect in a perturbation-theory approximation, they move apart on direct diagonalization of the appropriate Hamiltonian. The intersection of the energy levels leads to a discontinuity of the corresponding dipole-moment matrix element. The discontinuity of matrix elements is not reflected in the behaviour of transition probabilities which are continuous functions of the shape-anisotropy parameter. The profiles of a spectral line emitted or absorbed by an ensemble of ellipsoidally shaped nanoparticles with a Gaussian distribution of size are calculated and discussed.

© 2018 Association of Polish Electrical Engineers (SEP). Published by Elsevier B.V. All rights reserved.

1. Introduction

In a regime of strong size quantization, the electron-hole Coulomb interaction energy is much less than the energy of a charged-particle electron or hole confined within a crystalline semiconductor structure of varied shape and nanometre size. In this regime one can hence neglect the Coulomb interaction and treat the electron and hole independently. The most important result that early investigations revealed is the strong interdependence between the character of the energy spectrum of the nanometre-size object and its geometrical parameters [1]. In these works, the qualitative and quantitative descriptions of the electronic, optical and mechanical properties apply to spherical nanoparticles, i.e., for spherical quantum dots (see Ref. [2] and references therein). The properties of nanoparticles having cylindrical [3–6], ellipsoidal [7–10], semi-ellipsoidal [11], pyramidal and lens shape with infinite and finite [12–14] barrier heights were subsequently analysed. Furthermore, to facilitate the comparison of calculated results with the probable and available experimental data, size distribution of growing quantum dots have been taken into account [15–18].

Experiments indicate that small nanoparticles have a nearly spherical shape, whereas large nanoparticles have an ellipsoidal

shape. For the growth of a nanoparticle with various methods, the energy spectrum varies continuously with its size and shape. An advantage of nanoparticles of ellipsoidal shape with respect to spherical quantum dots arises from the additional geometrical characteristics related to shape-anisotropy parameter β ($\beta = c/a$ in which c and a are prolate ellipsoidal semi-axes). That effect makes possible the tuning of the spectral properties of objects of nanometre size. The tuneable control of spectral and optical characteristics of the nanometre objects through size and shape opens exciting possibilities for the engineering of new functional materials with a wide prospective application. Ellipsoidal nanoparticles thus play an important role for applications; the most promising candidates for further technological advances are precisely the ellipsoidally elongated objects of nanometre size. A comprehensive knowledge of the spectral and optical properties of ellipsoidally shaped nanoparticles is hence desirable.

In our recent papers [19,20], we considered a charged particle (electron or hole) confined within a potential well of ellipsoidal shape; the problem was solved in an effective-mass approximation. We assumed that a spherical potential well with infinitely high walls was subject to a deformation, which makes its shape that of a prolate ellipsoid. For a small deviation from the sphere the problem is solvable according to perturbation theory, with the unperturbed wave functions and energy levels corresponding to a spherical well. For an arbitrary deviation from a spherical shape the problem was solved using a direct diagonalization of the appropriate Hamiltonian. The energy levels and the corresponding wave functions have

* Corresponding author at: Faculty of Exact and Natural Sciences, Tbilisi State University, 0179 Tbilisi, Georgia.

E-mail address: tamaz.kereselidze@tsu.ge (T. Kereselidze).

been thus obtained for the shape-anisotropy parameter β over a wide range. Using the obtained wave functions and energy levels, we calculated the optical-transition matrix elements in the dipole approximation. The transition-matrix elements involving the ground and first excited states are monotonic functions of β , whereas matrix elements involving the corresponding excited states have zeros and extrema that are reflected in the behaviour of their transition probabilities. Furthermore, some matrix elements involving the highly excited states have a discontinuity. This outcome is unexpected and requires comprehensive study to establish its origin and influence on the optical properties of nanoparticles. Although the existence of an effect of quantum confinement on the optical response of nanoparticles is well established, the fine structure of their emission and absorption spectra is incompletely studied.

For a diatomic molecule, only terms of distinct symmetry can intersect; the intersection of terms of like symmetry is impossible [21]. If, as a result of some approximate calculation, we obtain two intersecting terms of the same symmetry, they are found to move apart on calculating the next level of approximation. This result not only is true for a diatomic molecule but also is a general theorem of quantum mechanics; it holds for any case in which the Hamiltonian contains some parameter of which its eigenvalues are consequently functions [22].

In this work, we seek to show that the above-mentioned property of diatomic quasi-molecules is also characteristic for ellipsoidally shaped nanoparticles with a variable parameter. Explicitly, we show that for an ellipsoidally shaped nanoparticle some curves representing the highly excited energy levels of the same symmetry intersect for the same shape-anisotropy parameter β if the energy levels are calculated with perturbation theory; the intersection of these curves is impossible if the energy levels are obtained by a direct diagonalization of the appropriate Hamiltonian, i.e., when the interaction between the states is fully taken into account. We demonstrate that the intersection of the excited energy levels of the same symmetry leads to the discontinuity of the dipole-moment matrix elements involving the excited and ground states. Moreover, we explore the optical properties and show that the appearance of some features in the profiles of spectral lines emitted or absorbed by an ensemble of ellipsoidally shaped nanoparticles is caused entirely by the existence of minima and zeros in the appropriate dipole-moment matrix elements.

The article is organized as follows. After stating the purpose, we present briefly the basic equations in Sect. 2. The results of calculations are presented and discussed in Sects. 3 and 4, before a conclusion in Sect. 5.

2. Intersecting and non-intersecting energy levels

We consider a charged particle of effective mass m^* confined within a potential well of ellipsoidal shape with semi-axes $a=b$ and c :

$$\frac{x^2+y^2}{a^2} + \frac{z^2}{c^2} = 1. \quad (1)$$

In (1) a represents the size of a well in directions x and y , c is the size in the direction z . The simplest potential $V(x, y, z)$ of that type is zero inside the ellipsoid and infinite on the surface of the ellipsoid and beyond. The corresponding Schrödinger equation that describes the motion of a particle trapped inside the ellipsoid, with the boundary condition for the wave function to be zero on the surface and outside the surface of the ellipsoid, reads:

$$\left[\Delta_{xyz} + K^2 - \frac{2m^*}{\hbar^2} V(x, y, z) \right] \Psi(x, y, z) = 0, \quad (2)$$

in which $K^2 = 2m^*E/\hbar^2$.

In new variables $\xi = xr_0/a$, $\eta = yr_0/a$ and $\zeta = zr_0/c$, the boundary condition transforms from the surface of the ellipsoid to the surface of a sphere of radius $r_0 = (\xi^2 + \eta^2 + \zeta^2)^{1/2}$. After writing the Laplace operator Δ_{xyz} in the new variables, we rewrite Eq. (2) as:

$$[\Delta_{\xi\eta\zeta} + K^2 - \alpha U(\xi, \eta, \zeta)] \Psi(\xi, \eta, \zeta) = 0, \quad (3)$$

in which

$$U = \begin{cases} \frac{c^2(a^2 - r_0^2)}{r_0^2(c^2 - a^2)} \Delta_{\xi\eta\zeta} + \frac{\partial^2}{\partial \zeta^2} & \text{if } \xi^2 + \eta^2 + \zeta^2 < r_0^2, \\ \infty & \text{if } \xi^2 + \eta^2 + \zeta^2 \geq r_0^2. \end{cases} \quad (4)$$

and $\alpha = r_0^2(c^2 - a^2)/(ac)^2$ is the parameter that reflects the deviation of the potential well from a spherical well. Parameter α is related to β according to $\alpha = r_0^2(1 - \beta^{-2})/a^2$.

Transforming from coordinates ξ , η and ζ to spherical coordinates $\xi = rsin\vartheta cos\varphi$, $\eta = rsin\vartheta sin\varphi$ and $\zeta = rcos\vartheta$ in Eqs. (3) and (4), we obtain an equation that describes the motion of a particle in the sphere:

$$[\Delta_{r\vartheta\varphi} + K^2 - \alpha U(r, \vartheta, \varphi)] \Psi(r, \vartheta, \varphi) = 0. \quad (5)$$

The problem of the motion of a charged particle in an ellipsoidal well thus reduces to the solutions of Eq. (5), in which effective potential $U(r, \vartheta, \varphi)$ is defined with Eq. (4) with $\Delta_{\xi\eta\zeta}$ replaced with the Laplace operator written in spherical coordinates, and $\partial/\partial\zeta = \partial/\partial r cos\vartheta - r^{-1} sin\vartheta \partial/\partial\vartheta$.

2.1. A perturbation approach

In a spherical potential well ($\alpha = 0$), the states of a particle are specified with quantum numbers n , l and m . Here l is the orbital quantum number and $m = 0, \pm 1, \pm 2, \dots$ is the magnetic quantum number of the particle; n , which has no dependence on m , numbers the level in the spherical well for given l . The solutions of equation $(\Delta_{r\vartheta\varphi} + k_{nl}^2)\psi_{nlm} = 0$ are well known and given in textbooks. The eigenfunctions are $\psi_{nlm}(r, \vartheta, \varphi) = C_{nl} j_l(k_{nl} r) Y_{lm}(\vartheta, \varphi)$, in which C_{nl} are normalizing factors, $j_l(k_{nl} r)$ are spherical Bessel functions and $Y_{lm}(\vartheta, \varphi)$ are spherical harmonics. The corresponding eigenvalues depend on the size of the potential well, r_0 , and two quantum numbers n and l : $k_{nl}^2 = \tau_{nl}^2/r_0^2$, in which τ_{nl} is the n th root of a spherical Bessel function determined from the condition $j_l(k_{nl} r_0) = j_l(\tau_{nl}) = 0$.

In Ref. [19] we assumed that αU is a small perturbation and solved Eq. (5) using perturbation theory. For the first-, second- and third-order corrections to the unperturbed energy, $E_{nl}^{(0)} = \hbar^2 \tau_{nl}^2/(2m^* r_0^2)$, we obtained:

$$\begin{aligned} E_{nlm} &= \left(\frac{r_0^2}{a^2} + \alpha E_{nlm}^{(1)} + \alpha^2 E_{nlm}^{(2)} + \alpha^3 E_{nlm}^{(3)} \right) E_{nl}^{(0)}, \\ E_{nlm}^{(1)} &= \frac{1 - 2l(l+1) + 2m^2}{(2l-1)(2l+3)}, \\ E_{nlm}^{(2)} &= A_{l+2}^2 B_{nl+2}^{(3)} + A_{l-2}^2 B_{nl-2}^{(3)}, \\ E_{nlm}^{(3)} &= \left(\frac{c^2(a^2 - r_0^2)}{r_0^2(c^2 - a^2)} - A_l \right) \left[A_{l+2}^2 B_{nl+2}^{(4)} + A_{l-2}^2 B_{nl-2}^{(4)} \right] \tau_{nl}^2. \end{aligned} \quad (6)$$

In Eq. (6) A_l and $A_{l\pm 2}$ are defined with expressions (A7) presented in Appendix A of Ref. [19]; $B_{nl\pm 2}^{(s)} = \sum_{n'} \tau_{n'l\pm 2}^2 / (\tau_{nl}^2 - \tau_{n'l\pm 2}^2)^s$ is the infinite sum; τ_{nl} and $\tau_{n'l\pm 2}$ are the roots of spherical Bessel functions $j_l(k_{nl} r)$ and $j_{l\pm 2}(k_{n'l\pm 2} r)$, respectively. For some states the energy levels calculated using Eq. (6) are given in Appendix A.

We introduce dimensionless quantity ε_{nlm} that is related to energy E_{nlm} through equation. Figure 1 shows ε_{131} , ε_{211} and ε_{151} as

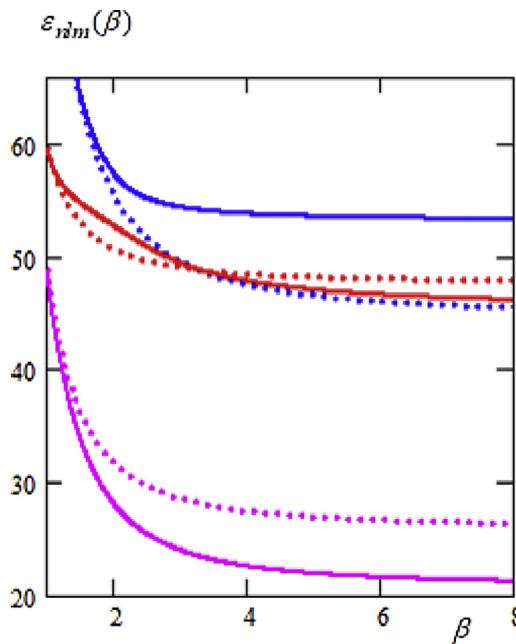


Fig. 1. Quantities ε_{131} (magenta dotted curve), ε_{211} (red dotted curve) and ε_{151} (blue dotted curve) as a function of β calculated using perturbation theory. The solid curves represent the same quantities but obtained from diagonalization of the Hamiltonian.

a function of shape-anisotropy parameter β . Dimensionless quantities ε_{nlm} were calculated using Eqs. (A.5), (A.7) and (A.9) in which the latter two terms were neglected. In these equations $a=r_0$ is fixed and c increases from $c=r_0$ up to $c=8r_0$. Figure 1 shows that the curves representing energy levels E_{211} and E_{151} intersect at $\beta=\beta_0=3.28$.

From equations presented in Appendix A follows that the perturbed energy levels other than E_{211} and E_{151} do not intersect.

2.2. Diagonalization of the Hamiltonian

We proceed to solve Eq. (5) by a direct diagonalization of the Hamiltonian $H=H_0+\alpha\hbar^2U/2m^*$ in which $H_0=-\hbar^2\Delta_{r\vartheta\varphi}/2m^*$, $U=\partial^2/\partial z^2$ and $\partial/\partial\zeta=\partial/\partial r\cos\vartheta-r^{-1}\sin\vartheta\partial/\partial\vartheta$ ($a=r_0$ in Eq. (4)). An analysis of the roots of the Bessel functions yields the following series of energy levels in the spherical well: 1s, 1p, 1d, 2s, 1f, 2p, 1g, 2d, 1h, ... (s, p, d, \dots denote energy levels with angular momentum quantum number $l=0, 1, 2, \dots$ [22]). For our purpose it is more convenient to consider the states with given m separately and to enumerate the states as follows: $\psi_1\equiv\psi_{10m}$, $\psi_2\equiv\psi_{12m}$, $\psi_3\equiv\psi_{20m}$, $\psi_4\equiv\psi_{14m}, \dots$ and analogously $\psi_1\equiv\psi_{11m}$, $\psi_2\equiv\psi_{13m}$, $\psi_3\equiv\psi_{21m}$, $\psi_4\equiv\psi_{15m}, \dots$ We hence introduce states in two sets with even and odd l . Taking into account that the matrix element $\langle\psi_{nlm}|U|\psi_{n'l'm}\rangle$ differs from zero if $|l|=l\pm 2$ [19], one obtains that the introduced sets of wave functions are not bound; the states with even and odd l can hence be considered independently.

We seek the solutions of Eq. (4) with a given parity of l as follows:

$$\Psi_i(r, \vartheta, \varphi) = \sum_{j=1}^4 C_j(E_i) \psi_j(r, \vartheta, \varphi). \quad (7)$$

In Eq. (7) C_j are expansion coefficients that depend on energy E_i of the i th state.

The solution of Eq. (5) we thus reduce to the solution of a system of homogeneous linear equations:

$$2m^*\hbar^{-2}(E - \tilde{U}_{11})C_1 - \alpha U_{12}C_2 = 0,$$

$$\alpha U_{21}C_1 - 2m^*\hbar^{-2}(E - \tilde{U}_{22})C_2 + \alpha U_{23}C_3 + \alpha U_{24}C_4 = 0, \quad (8)$$

$$\alpha U_{32}C_2 - 2m^*\hbar^{-2}(E - \tilde{U}_{33})C_3 = 0,$$

$$\alpha U_{42}C_2 - 2m^*\hbar^{-2}(E - \tilde{U}_{44})C_4 = 0,$$

in which $\tilde{U}_{ii} = E_i^{(0)} + \alpha\hbar^2U_{ii}/2m^*$, U_{ij} are the matrix elements of the operator U with respect to the unperturbed wave functions $\psi_i\equiv\psi_{nlm}$; $E_i^{(0)}=E_{nl}^{(0)}$ are the energy levels of a charged particle trapped in the spherical potential well.

The consideration of only four states in Eq. (7) is stipulated by the fact that in this case the equation for the energy arises of the fourth degree, which can be solved algebraically using the Ferrari method [23]. The four-state approximation can reproduce satisfactorily accurately all levels of an ellipsoidal nanoparticle that correspond to the spherical quantum-dot levels specified at the beginning of this subsection (an exception is level 2d with $m=0$, which should be treated in a five-state approximation).

In Figure 1 the solid curves represent dimensionless quantities $\varepsilon_2=2m^*r_0^2E_2/\hbar^2$, $\varepsilon_3=2m^*r_0^2E_3/\hbar^2$ and $\varepsilon_4=2m^*r_0^2E_4/\hbar^2$ that are obtained from the solution of the secular equation (the equation derived from the condition that the determinant of the coefficients of the unknowns in Eq. (8) vanishes). Figure 1 shows that the solid curves do not intersect. We thus obtained that, in accordance with the general theorem of quantum mechanics, the intersecting energy levels of the same symmetry move apart on calculating the next approximation. In the present case, the non-crossing of the energy levels is caused by the interaction of $\psi_{21\pm 1}$ and $\psi_{15\pm 1}$ states with third state $\psi_{13\pm 1}$, rather than a result of the direct interaction of $\psi_{21\pm 1}$ and $\psi_{15\pm 1}$ states ($U_{34}=U_{43}=0$ in Eq. (8)). Another characteristic that follows from Figure 1 is that for $\beta=\beta_0$, energy level E_3 obtained on diagonalizing the Hamiltonian coincides with the energy levels $E_{21}^{(0)}+\alpha\hbar^2U_{33}/2m^*$ and $E_{15}^{(0)}+\alpha\hbar^2U_{44}/2m^*$ calculated using perturbation theory.

3. Discontinuity of the dipole-moment matrix elements

After analysis of the energy spectrum, we derive the matrix elements of electric dipole moment $\vec{d}=e\vec{r}$ with respect to wave functions (7); e is the charge and \vec{r} is the position vector of a particle trapped in the ellipsoid. Specifically, we derive the matrix elements of operators $d_{\pm}=2^{-1/2}(x\pm iy)/r_0$ and $d_z=z/r_0$, which determine the circularly and linearly polarized radiation, respectively. Because the integrals from the normalized spherical Bessel functions are proportional to r_0 , the calculated matrix elements are independent of the size of the sphere for which the integration is implemented.

In Appendix B we present explicit expressions for expansion coefficients $C_j(E_i)$ in Eq. (7) obtained from the solution of system of homogeneous linear equations (8). The derived expressions show that expansion coefficients $C_1(E_3)$, $C_3(E_3)$ and $C_4(E_3)$ have a singularity when $E_3=\tilde{U}_{11}$, $E_3=\tilde{U}_{33}$ and $E_3=\tilde{U}_{44}$. In Sect. 2, we revealed that $E_3\neq\tilde{U}_{11}$ for an anisotropy parameter of arbitrary shape, whereas $E_3=\tilde{U}_{33}=\tilde{U}_{44}$ for $\beta=\beta_0$ (see Figure 1). Unnormalized wave function $\Psi_3(r, \vartheta, \varphi)$ has hence a singularity for $\alpha_0=1-\beta_0^{-2}$, which vanishes after normalization. A small calculation confirms that, in the vicinity of α_0 , $\Psi_3(r, \vartheta, \varphi)$ takes the form:

$$\Psi_3(r, \vartheta, \varphi) = \frac{|\alpha-\alpha_0|}{\alpha-\alpha_0} \frac{U_{32}\psi_3+U_{42}\psi_4}{\sqrt{U_{32}^2+U_{42}^2}}. \quad (9)$$

We thus obtain that normalized wave function $\Psi_3(r, \vartheta, \varphi)\equiv\Psi_{21\pm 1}(r, \vartheta, \varphi)$ has a discontinuity, which in turn leads to a discontinuity of the dipole-moment matrix elements derived using this wave function. Figures 2(a) and 2(b) show dipole-moment

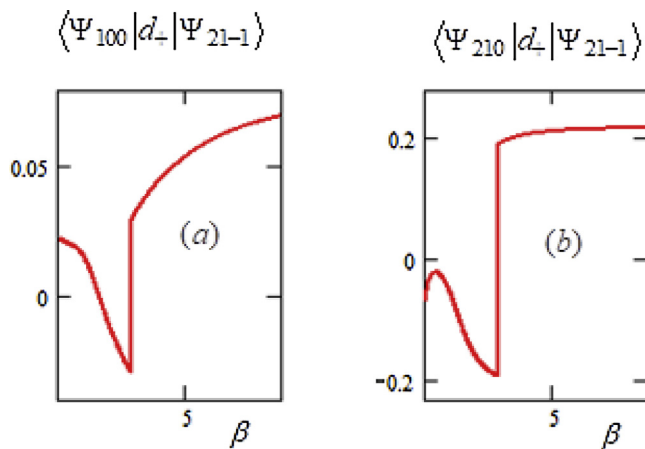


Fig. 2. The dipole moment matrix elements as a function of β .
(a) – $\langle \Psi_{100} | d_+ | \Psi_{21-1} \rangle$ and (b) – $\langle \Psi_{120} | d_+ | \Psi_{21-1} \rangle$.

matrix elements $\langle \Psi_{100} | d_+ | \Psi_{21-1} \rangle$ and $\langle \Psi_{120} | d_+ | \Psi_{21-1} \rangle$ as a function of β . These figures clearly show that both matrix elements have a discontinuity for $\beta = \beta_0$. The magnitudes of the left and right parts of the dipole-moment matrix elements coincide at $\beta = \beta_0$ but have opposite signs.

We introduce the oscillator strength [24]:

$$F_f i = (2m^* r_0 \hat{2}) / \hbar \hat{2} (E_i - E_f) |f| d_{(\pm, z)} |i\rangle |\hat{2}| \quad (10)$$

which is a dimensionless quantity that expresses the probability of emission and absorption of electromagnetic radiation in transitions between energy levels E_i and E_f of a nanoparticle.

In the dipole approximation, the transition probability during unit time from an initial state $|i\rangle$ to a final state $|f\rangle$ is proportional to the quantity [24]:

$$W_{fi} = \frac{\hbar}{4\pi m^* c^2} \left(\frac{e^2}{\hbar c} \right) \omega_{if}^2 F_{fi}, \quad (11)$$

in which

$$\omega_{if} = \frac{\hbar}{2m^* r_0^2} (\varepsilon_i - \varepsilon_f) \equiv \frac{\hbar}{2m^* r_0^2} \varepsilon_{if}(\beta) \quad (12)$$

is the transition frequency corresponding to given shape-anisotropy parameter β .

Figure 3 shows the interband electron-transition probabilities as a function of β calculated for an ellipsoidally shaped nanoparticle of ZnO using dipole-moment matrix elements $\langle \Psi_{100} | d_+ | \Psi_{21-1} \rangle$ and $\langle \Psi_{120} | d_+ | \Psi_{21-1} \rangle$. The small semi-axis of the ellipsoid is fixed at $a = r_0 = 1$ nm; the effective mass is $m^* = 0.24 m_e$ with electron mass m_e . Figure 3 shows that transition probabilities $W_{100,21-1}$ and $W_{120,21-1}$ are continuous functions of the shape-anisotropy parameter in the entire region of β including the vicinity of point $\beta = \beta_0$ (the discontinuities disappear because transition probabilities are proportional to the squared modulus of the transition dipole moment). Figure 3 shows also that $W_{100,21-1}$ is equal to zero for $\beta = 2.29$ and $W_{120,21-1}$ becomes small when $\beta = 1.29$.

4. Profiles of spectral lines

The system of nanoparticles is generally inhomogeneous because the particle size varies greatly. The results of calculations of the absorption coefficients of non-uniform nanoparticle ensembles are reported in the literature. However, a realistic approach for interband transitions considering the size distribution of nanoparticles is not yet developed.

In this section, we calculate the profile of a spectral line emitted or absorbed by an ensemble of ellipsoidal shaped nanoparticles. The

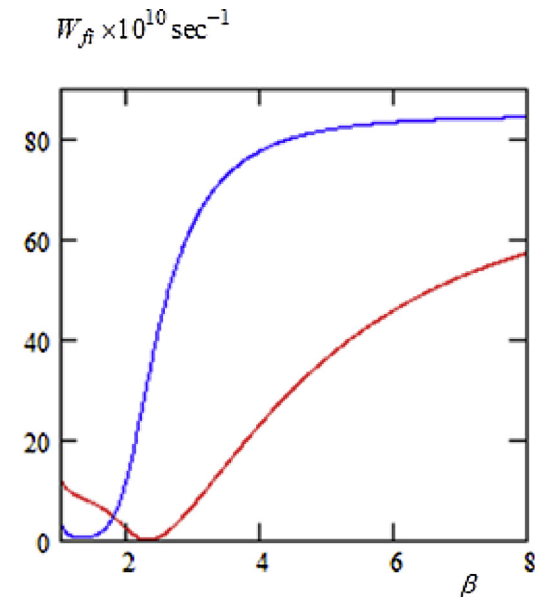


Fig. 3. Interband transition probabilities $W_{100,21-1}$ (red curve) and $W_{120,21-1}$ (blue curve) as a function of β calculated for a ZnO nanoparticle using Eq. (11); $W_{120,21-1}$ is divided by 5.

observed optical spectra are considered as a superposition of the contributions from each individual nanoparticle in the ensemble. Although both Gaussian and Lorentzian distribution functions are reported in the literature [15–18], the experimental work [25,26] indicates Gaussian distributions.

If ellipsoidally shaped nanoparticles are statistically distributed about mean shape-anisotropy parameter $\bar{\beta}$ according to a Gaussian function, one can write that [18]:

$$n(\beta) = De^{-\frac{(\beta-\bar{\beta})^2}{2s^2}}, \quad (13)$$

in which s is the standard deviation of the Gaussian function; $n(\beta)$ is the normalized with the condition:

$$\int_1^\infty n(\beta)d\beta = 1. \quad (14)$$

Introducing the relative standard deviation of the Gaussian function as $\mu = s/\bar{\beta}$, we obtain:

$$n(\beta) = De^{-\frac{(\beta/\bar{\beta}-1)^2}{2\mu^2}}. \quad (15)$$

The explicit expression for normalizing factor D is given in Appendix C.

For ellipsoidally shaped nanoparticles with shape-anisotropy parameter β lying in a given interval $d\beta$, the total transition probability during unit time from initial state $|i\rangle$ to final state $|f\rangle$ is:

$$I_{fi}(\beta)d\beta = W_{fi}(\beta)n(\beta)d\beta, \quad (16)$$

in which $W_{fi}(\beta)$ is defined with Eq. (11).

Further, rewriting Eq. (16) as:

$$I_{fi}(\beta)d\beta = W_{fi}(\beta)n(\beta) \frac{d\beta}{d\omega_{if}} d\omega_{if} \equiv I(\omega_{if})d\omega_{if}, \quad (17)$$

we obtain a profile of a spectral line as:

$$I(\omega_{if}) = \frac{W_{fi}(\omega_{if})n(\omega_{if})}{|\frac{d\omega_{if}}{d\beta}|}. \quad (18)$$

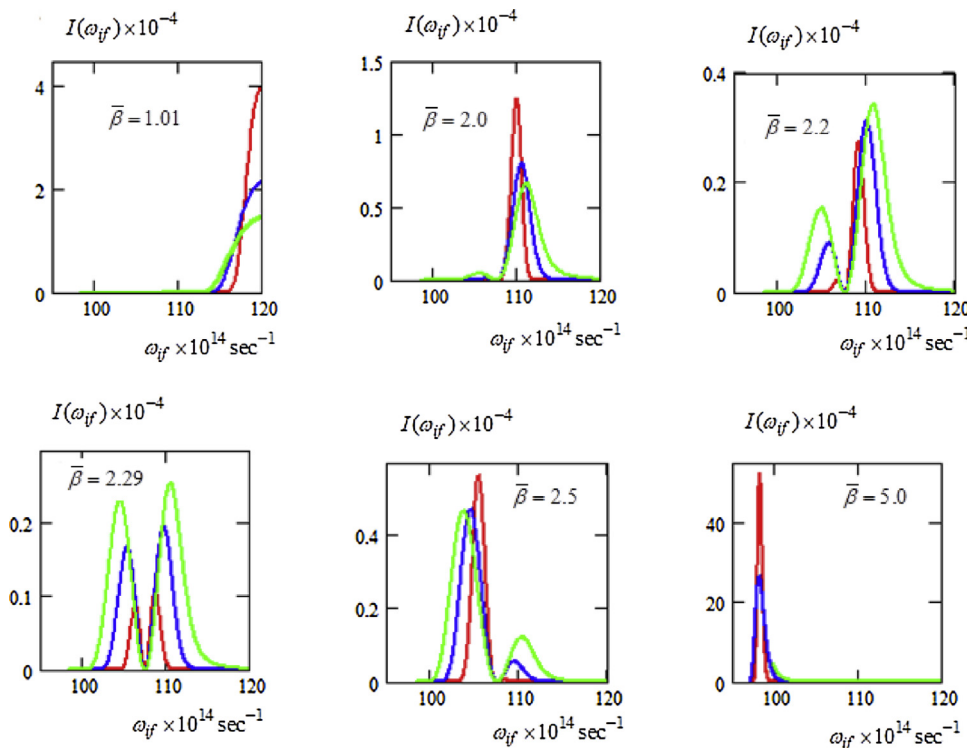


Fig. 4. Profiles of spectral lines for transitions between excited state Ψ_{21-1} and the ground state calculated for the ensembles of ZnO nanoparticles; red curves – $\mu = 0.05$, blue curves – $\mu = 0.10$ and green curves – $\mu = 0.15$.

The dependence of transition frequency ω_{if} on β is determined with Eq. (12); hence:

$$\left| \frac{d\omega_{if}}{d\beta} \right| = \left(\frac{\hbar}{2m^*r_0^2} \right) \left| \frac{d\varepsilon_{if}}{d\beta} \right|, \quad (19)$$

in which $|d\varepsilon_{if}/d\beta|$ is calculated for β corresponding to the given transition frequency.

Using Eqs. (11), (15), (18) and (19), we calculated the profiles of spectral lines for interband optical transitions of ensembles of ellipsoidally shaped ZnO nanoparticles. Calculations were performed for the transitions between excited state Ψ_{12-1} and ground state Ψ_{100} of nanoparticles with varied mean shape-anisotropy parameter $\bar{\beta}$ and relative standard deviation μ ; the results appear in Figure 4. These profiles depend strongly on both the size of the nanoparticle ($\bar{\beta} = \bar{c}/a$ in which $a = r_0 = 1 \text{ nm}$) and relative standard deviation μ . Explicitly, there is one maximum for almost spherical shaped nanoparticles ($\bar{\beta} = 1.01$), whereas two maxima appear for ellipsoidally shaped nanoparticles with $1.5 < \bar{\beta} < 3.0$. For nanoparticles with a strongly prolate ellipsoidal shape ($\bar{\beta} > 5.0$) there is again one maximum. The left maximum thus increases and the right maximum decreases with increasing size of the nanoparticle, which indicates a red shift of the line profiles. Increasing relative standard deviation $\xi \mu$ alters the magnitude of maxima and leads to the broadening of line profiles.

Figure 5 elucidates the appearance of two maxima in the profile of a spectral line for $\bar{\beta} = 2.29$, i.e., when dipole-moment matrix element $\langle \Psi_{100} | d_+ | \Psi_{21-1} \rangle$ is zero [see Figure 2(a)].

5. Conclusions

In this work, we consider a charged particle confined within an ellipsoidally shaped potential well with infinitely high walls. Using this model, we have analysed the optical properties of crystalline

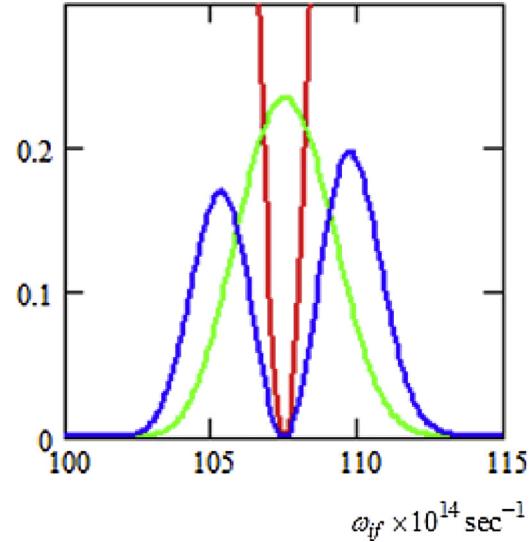


Fig. 5. As in Figure 4, but for $\bar{\beta} = 2.29$ and $\mu = 0.1$; red curve – $W_{fi}(\omega_{if}) \times 10^{10} \text{ sec}^{-1}$, green curve – $-n(\omega_{if})|d\omega_{if}/d\beta|^{-1} 5.788 \times 10^{13} \text{ sec}^{-1}$ and blue curve – $I(\omega_{if}) \times 10^{-4}$.

semiconductor objects with ellipsoidal shape and nanometre size. The optical transition-matrix elements have been calculated in a dipole approximation as a function of shape-anisotropy parameter β using perturbation theory and with a direct diagonalization of the appropriate Hamiltonian. Matrix elements $\langle \Psi_{100} | d_+ | \Psi_{21-1} \rangle$ and $\langle \Psi_{120} | d_+ | \Psi_{21-1} \rangle$ are shown to be discontinuous, which is caused by the intersection of energy levels of the same symmetry calculated with perturbation theory (the intersecting energy levels move apart on calculating with a direct diagonalization of the Hamiltonian). The discontinuity of the matrix elements is not reflected

in the behaviour of transition probabilities, which are continuous functions of the shape-anisotropy parameter.

We investigated the effect of size non-uniformity on the profiles of spectral lines of ZnO nanoparticles with a size distribution described with a Gaussian function. The line profiles depend strongly on the shape-anisotropy parameter; the appearance of structure in the line profiles is entirely caused by the existence of zeros and minima in the dipole-moment matrix elements. In the Gaussian function, increasing relative standard deviation $\xi \mu$ alters the magnitude of maxima and leads to broadened spectral lines. The revealed optical properties make attractive ellipsoidally elongated objects of nanometre size for various applications, such as infrared detectors.

In our calculations of the profiles of spectral lines, we applied the ellipsoidally shaped potential well with infinitely high walls, which makes difficult achievement of agreement with the reported experimental results. Calculations with the ellipsoidally shaped potential well with finite walls are at present under consideration.

Acknowledgement

Shota Rustaveli Georgian National Science Foundation and Science and Technology Center in Ukraine (No 0404, No 6207) jointly supported this research.

Appendix A.

Energy levels of some states were calculated with Eq. (6) and $a = r_0$:

$$2m^*r_0^2E_{100}/\hbar^2 = (1 - 0.3333\alpha - 0.0093\alpha^2 + 0.0012\alpha^3) 9.8697, \quad (\text{A.1})$$

$$2m^*r_0^2E_{110}/\hbar^2 = \{1 - 0.6\alpha - 0.0158\alpha^2 + 0.0062\alpha^3\} 20.1906, \quad (\text{A.2})$$

$$2m^*r_0^2E_{111}/\hbar^2 = (1 - 0.2\alpha - 0.0105\alpha^2 + 0.0014\alpha^3) 20.1906, \quad (\text{A.3})$$

$$2m^*r_0^2E_{130}/\hbar^2 = \{1 - 0.5111\alpha - 0.3516\alpha^2 + 0.7637\alpha^3\} 48.8307, \quad (\text{A.4})$$

$$2m^*r_0^2E_{131}/\hbar^2 = (1 - 0.4667\alpha - 0.2424\alpha^2 + 0.4685\alpha^3) 48.8307, \quad (\text{A.5})$$

$$2m^*r_0^2E_{210}/\hbar^2 = (1 - 0.6\alpha + 0.2551\alpha^2 + 0.8707\alpha^3) 59.6787, \quad (\text{A.6})$$

$$2m^*r_0^2E_{211}/\hbar^2 = (1 - 0.2\alpha + 0.1700\alpha^2 + 0.1935\alpha^3) 59.6787, \quad (\text{A.7})$$

$$2m^*r_0^2E_{150}/\hbar^2 = (1 - 0.5043\alpha - 0.1035\alpha^2 + 0.1165\alpha^3) 87.5310, \quad (\text{A.8})$$

$$2m^*r_0^2E_{151}/\hbar^2 = (1 - 0.4872\alpha + 0.0023\alpha^2 + 0.1037\alpha^3) 87.5310, \quad (\text{A.9})$$

Appendix B.

In the four-state approximation, normalized wave functions $\Psi_i(r, \vartheta, \varphi)$ ($i = 1, 2, 3, 4$) are represented as

$$\Psi_i = C(C_1\Psi_1 + \Psi_2 + C_3\Psi_3 + C_4\Psi_4), \quad (\text{B.1})$$

in which

$$C_1 = \frac{\alpha\hbar^2U_{12}}{2m^*(E_i - \tilde{U}_{11})},$$

$$C_3 = \frac{\alpha\hbar^2U_{32}}{2m^*(E_i - \tilde{U}_{33})}, \quad (\text{B.2})$$

$$C_4 = \frac{\alpha\hbar^2U_{42}}{2m^*(E_i - \tilde{U}_{44})},$$

$$C = \left\{ 1 + \left(\frac{\alpha\hbar^2}{2m^*} \right)^2 \left[\left(\frac{U_{12}}{E_i - \tilde{U}_{11}} \right)^2 + \left(\frac{U_{32}}{E_i - \tilde{U}_{33}} \right)^2 + \left(\frac{U_{42}}{E_i - \tilde{U}_{44}} \right)^2 \right] \right\}^{-1/2};$$

E_i are the roots obtained from the solution of the secular equation. Explicit expressions for E_i are presented in Appendix B of reference [19].

Appendix C.

Integral Eq. (14) with $n(\beta)$ defined according to Eq. (13) can be reduced to tabulated integrals. A small calculation of the normalizing factor in Eq. (13) yields:

$$D = \frac{1}{\sqrt{2}\beta\mu} \left(\frac{\sqrt{\pi}}{2} + \chi(v) \right)^{-1}, \quad (\text{C.1})$$

in which $v = 2^{-1/2}(\beta - 1)/(\beta\mu)$ and [27]

$$\chi(v) = v \left(1 - \frac{v^2}{1!3} + \frac{v^4}{2!5} - \frac{v^6}{3!7} + \dots \right) \quad (\text{C.2})$$

for $v < 1$,

$$\chi(v) = \frac{\sqrt{\pi}}{2} \left[1 - \frac{e^{-v^2}}{v\sqrt{\pi}} \left(1 - \frac{1}{2v^2} + \frac{1 \cdot 3}{2^2 v^4} - \frac{1 \cdot 3 \cdot 5}{2^3 v^6} + \dots \right) \right] \quad (\text{C.3})$$

for $v > 1$.

References

- [1] P. Harrison, *Quantum Well, Wires and Dots*, Wiley, New York USA, 2005.
- [2] T. Chakraborty, *Quantum Dots: A Survey of the Properties of Artificial Atoms*, Elsevier, Science, Amsterdam, Netherlands, 1999.
- [3] M. Kuno, *Introductory Nanoscience*, Garland Science, London, UK and New York, USA, 2012.
- [4] K. Warda, The size effect in the equation of state for nanostructures, *J. Phys.: Condens. Matter* 21 (2009) 345301.
- [5] A. Shabaev, Al. L. Efros, 1D Exciton Spectroscopy of Semiconductor Nanorods, *Nano Lett.* 4 (2004) 1821.
- [6] B. Zh. Pogosyan, G.H. Demitjian, Binding energy of hydrogenic impurities in quantum well, wires of InSb/GaAs, *Physica B* 338 (2003) 357.
- [7] G. Cantele, D. Ninno, G. Iadonisi, Calculation of the Infrared Optical Transitions in Ellipsoidal Quantum Dots, *Nano Lett.* 1 (2001) 121.
- [8] G. Cantele, D. Ninno, G. Iadonisi, Shape effects on the one- and two-electron ground state in ellipsoidal quantum dots, *Phys. Rev. B* 64 (2001) 125325.
- [9] G. Cantele, G. Piacente, D. Ninno, G. Iadonisi, Optical anisotropy of ellipsoidal quantum dots, *Phys. Rev. B* 66 (2002) 113308.
- [10] D.A. Bagdasaryan, D.B. Hayrapetyan, E.M. Kazaryan, Prolate spheroidal quantum dot: Electronic states, direct interband light absorption and electron dipole moment, *Physica B* 479 (2015) 85.
- [11] H. Leon, J.L. Marin, R. Riera, Excitonic and electronic states in ellipsoidal and semielipsoidal quantum dots, *Physica E* 27 (2005) 385.
- [12] A. Bagga, S. Ghosh, P.K. Chattopadhyay, Energy levels in spheroidal quantum dots with finite, barrier heights, *Nanotechnology* 16 (2005) 2726.
- [13] A.A. Gusev, O. Chuluunbaatar, S.I. Vinitsky, K.G. Dvoyan, E.M. Kazaryan, H.A. Sarkisyan, V.L. Devrob, A.S. Klobotskaya, V.V. Serov, Adiabatic description of nonspherical quantum dot models, *Yad. Fiz.* 75 (2012) 1281.
- [14] T. Kereselidze, T. Tchelidze, T. Nadareishvili, R. Ya Keserashvili, spectra of a particle, confined in a finite ellipsoidal shaped potential well, *Physica E* 81 (2016) 196.
- [15] D.L. Ferreira, J.L.A. Alves, The effects of shape and size nonuniformity on the absorption, spectrum of semiconductor quantum dots, *Nanotechnology* 15 (2004) 975.
- [16] S. Kumar, D. Biswas, Effect of a Gaussian size distribution on the absorption spectra of III-V semiconductor quantum dots, *J. Appl. Phys.* 102 (2007) 084305.
- [17] K.G. Dvoyan, D.B. Hayrapetian, E.M. Kazaryan, Direct Interband Light Absorption in Strongly Prolated Ellipsoidal Quantum Dots' Ensemble, *Nanoscale Res. Lett.* 4 (2009) 106.
- [18] S. Kabi, A.G. Unil Perera, Effect of quantum dot size and size distribution on the intersublevel, transitions and absorption coefficients of III-V semiconductor quantum dot, *J. Appl. Phys.* 117 (2015) 124303.
- [19] T. Kereselidze, T. Tchelidze, R. Ya Keserashvili, Energy levels of a particle confined in an, ellipsoidal potential well, *Physica E* 68 (2015) 65.
- [20] T. Kereselidze, T. Tchelidze, A. Devdariani, Interband optical transitions in ellipsoidal shaped, nanoparticles, *Physica B* 511 (2017) 36.
- [21] J. von Neumann, E.P. Wigner, Über das Verhalten von Eigenwerten bei adiabatischen Prozessen, *Phys. Z.* 30 (1929) 467.
- [22] L.D. Landau, E.M. Lifshitz, *Quantum mechanics: Non-Relativistic Theory*, Elsevier, Singapore, 2007.
- [23] A.G. Kurosh, *Course of Higher Algebra*, Gostekhizdat, Moscow, USSR, 1952.

- [24] N.A. Bethe, E.E. Salpeter, *Quantum Mechanics of One and Two-Electron Atoms*, Springer-Verlag, Berlin, Germany, 1957.
- [25] Q.D. Zhuang, J.M. Li, Y.P. Zeng, L. Pan, H.X. Li, M.Y. Kong, L.Y. Lin, Structural, characterization of InGaAs/GaAs quantum dots superlattice infrared photodetector structures, *J. Cryst. Growth* 200 (1999) 375.
- [26] K. Yamaguchi, K. Yujobo, T. Kaizu, Stranski-Krastanov growth of InAs quantum dots with narrow size distribution, *Jpn. J. Appl. Phys.* 39 (2000) L1245.
- [27] H.B. Dwight, *Tables of Integrals and Other Mathematical Data*, MacMillan, New York, USA, 1961.